Piezomodulated reflectivity of asymmetric and symmetric $Al_{x_1}Ga_{1-x_1}As/GaAs/Al_{x_3}Ga_{1-x_3}As$ single quantum wells

C. Parks, R. G. Alonso, and A. K. Ramdas
Department of Physics, Purdue University, West Lafayette, Indiana 47907

L. R. Ram-Mohan and D. Dossa
Department of Physics, Worcester Polytechnic Institute, Worcester, Massachusetts 01609

M. R. Melloch
School of Electrical Engineering, Purdue University, West Lafayette, Indiana 47907
(Received 20 January 1992)

The piezomodulated reflectivity spectra of compositionally asymmetric $Al_{x_1}Ga_{1-x_1}As$ / GaAs / $Al_{x_3}Ga_{1-x_3}As$ single quantum wells exhibit transitions from bound to quasibound and quasibound to quasibound states. The quasibound states, which exist in the continuum between the lower and upper barrier energies, participate resonantly in interband transitions. The piezomodulated reflectivity spectrum of an asymmetric quantum well designed with the appropriate parameters shows the absence of a bound state. Symmetric quantum wells are compared with their asymmetric counterparts of equal well width. When 1*s* and 2*s* excitonic signatures are observed, their separation is used to determine excitonic corrections.

I. INTRODUCTION

As is well known, the quantum confined states of symmetric single quantum wells grown by molecular-beam epitaxy (MBE) have quantized energies below the confining barrier potential. In addition, it has been recognized that for energies above the barrier potential, the continuum states exhibit quantum effects. These effects have been explored theoretically[1,2] and observed in photoluminescence excitation spectroscopy.[3–5] The piezomodulation technique has proved to be a valuable method for optically investigating quantum-confined transitions in MBE-grown heterostructures. This technique allows the observation of quantum-confined transitions from the valence-band to conduction-band states in addition to those corresponding to transitions from confined states in the spin-orbit split-off band to the conduction band.[6,7] It also has been recently shown to be a valuable tool for observing transitions involving quasibound resonant states.[8]

In this paper we examine "above-barrier" optical transitions in $Al_{x_1}Ga_{1-x_1}As/GaAs/Al_{x_3}Ga_{1-x_3}As$ compositionally asymmetric single quantum wells investigated with piezomodulation spectroscopy. The asymmetric wells have unequal barrier potential heights of V_1 and V_3 for the Al-Ga-As layers and $V_2 = 0$ (i.e., $x_2 = 0$) for the GaAs layer as depicted in Fig. 1. In particular, we observe the presence of quasibound resonant states existing in the continuum between the barrier energies in both the conduction and the valence bands. These states participate resonantly in optical transitions from bound to quasibound states as well as quasibound to quasibound states.

We have investigated the quasibound states in asymmetric quantum wells of widths 100, 50, 33, and 20 Å and compared the results with their symmetric counterparts of equal widths. The asymmetric quantum well 20 Å in width was designed with the appropriate parameters[9] to show the *absence* of a bound state, in contrast to symmetric quantum wells, which are required to possess at least one bound state.

II. EXPERIMENT

The quantum-well structures investigated in this work were grown in a Varian GEN II molecular-beam epitaxy (MBE) system on two-inch diameter, undoped, liquid-encapsulated-Czochralski-grown (100) GaAs substrates. The substrates were degreased, etched in a 60 °C solution of 5:1:1 of H_2SO_4:H_2O_2:H_2O for 1 min and placed in a

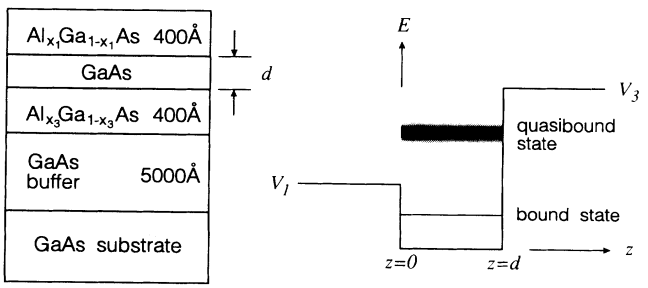

FIG. 1. A plot of the potential profile of an asymmetric $Al_{x_1}Ga_{1-x_1}As/GaAs/Al_{x_3}Ga_{1-x_3}As$ single quantum well.

nonbonded substrate mount. The substrates were outgassed for 2 h at 200 °C in the entry chamber of the MBE and then moved to the buffer chamber. Each substrate was outgassed for 1 h at 300 °C in the buffer chamber immediately before being loaded into the growth chamber. In the growth chamber, each sample was heated to 615 °C for 2 min (the surface oxides desorbed at 580 °C) and then the substrate temperature was lowered to the growth temperature of 600 °C. The films were grown using the tetramer arsenic source As_4, and two gallium effusion furnaces were utilized. Initially, a 0.5-μm GaAs buffer layer was grown at a growth rate of 1 μm/h and an As_4 to Ga beam-equivalent pressure of 15. This was followed by either a symmetric or asymmetric single-quantum-well structure. The single quantum wells ranged in width from 20 to 100 Å. The symmetric single-quantum-well structures possess 400-Å $Al_{0.3}Ga_{0.7}As$ barrier layers. The asymmetric single-quantum-well structures have a 400-Å $Al_{0.1}Ga_{0.9}As$ lower barrier and a 400-Å $Al_{0.3}Ga_{0.7}As$ upper barrier. The $Al_{0.3}Ga_{0.7}As$ barriers were grown using just one Ga effusion furnace while the $Al_{0.1}Ga_{0.9}As$ were grown by using two Ga effusion furnaces. There were 30-s growth interruptions upon completing growth of the first $Al_{0.3}Ga_{0.7}As$ layer and upon completing growth of the GaAs quantum well. The growth interruptions provide for smooth interfaces and a uniform thickness quantum well.

The piezomodulated reflectivity spectrum of the single quantum wells was achieved by fixing the GaAs substrate to a lead zirconate titanate transducer driven by a 560-V sinusoidal electric field. The alternating expansion and contraction of the transducer induced a rms strain of $\sim 10^{-5}$. A Janis Super Vari-Temp optical cryostat was employed with liquid helium as a coolant. The light source consisted of a tungsten halogen lamp which was passed through a Perkin-Elmer (model E-1) double-pass grating monochromator. A uv-enhanced Si photodiode detected the reflected light. The modulated component (ΔR) of the reflected spectrum was isolated by a lock-in amplifier. The operation of the monochromator and collection of the data were carried out with a microcomputer.

III. THEORY

A. Bound states

We consider planar layered semiconductor heterostructures with the planes perpendicular to the growth direction z. The layers are taken to be composed of compound III-V or II-VI semiconductors with their conduction- and valence-band edges located at the Γ point in the Brillouin zone. The periodic component of the Bloch functions, $u_{j,\mathbf{k}=0}(\mathbf{r})$ with j being the band index, at the band edges are assumed not to differ much as we traverse layer interfaces.[10] We assume that the original bulk crystal translational symmetry is maintained in the transverse direction.

We consider the zone-center bulk band structure of the constituent semiconductors, within the spirit of the $\mathbf{k}\cdot\mathbf{p}$ model. The usual eight-band model consists of the Γ_6 conduction band (c), the Γ_8 heavy-hole (hh) and light-hole (lh) bands, and the Γ_7 spin-orbit split-off band (s.o.), with their spin degeneracies. In the following, we limit ourselves to the case with no external electric or magnetic fields or built-in strain in the layers. The following considerations hold for the more general case with external perturbations except that the Kramers's degeneracy of the bands gets lifted, and the dimensions of the matrices are larger. The latter would be true also in the presence of strain. With this degeneracy and with the in-plane wave vector $(k_x, k_y) = 0$, the problem reduces to a three-band model, with the hh band factoring out. The problem of solving for the envelope functions of the constituent layers, within the envelope-function approximation, then reduces to the solution of a set of three simultaneous second-order differential equations for the envelope functions. We have

$$H_{ij}(k_\perp, k_z) f_j(z) = E f_i(z), \tag{1}$$

where k_z has to be replaced by the differential operator $-i\frac{\partial}{\partial z}$, and $\mathbf{k}_\perp = (k_x, k_y)$ is the in-plane wave vector which is set to zero in the following.

The eigenvalues of the 3×3 matrix are given by the secular equation (in atomic units)

$$\begin{vmatrix} E_c + (F+\frac{1}{2})k_z^2 - E & -\sqrt{E_P/3}k_z & -\sqrt{E_P/6}k_z \\ -\sqrt{E_P/3}k_z & E_v - \frac{1}{2}(\gamma_1 + 2\gamma_2)k_z^2 - E & -\sqrt{2}\gamma_2 k_z^2 \\ -\sqrt{E_P/6}k_z & -\sqrt{2}\gamma_2 k_z^2 & E_s - \frac{1}{2}\gamma_1 k_z^2 - E \end{vmatrix} = 0. \tag{2}$$

Here E_c, E_v, and E_s are the band-edge energies of the conduction, lh and the s.o. bands. The three coupled second-order differential equations represented by Eq. (1) can be written as

$$\left(-\mathcal{A}_{ab}\frac{\partial^2}{\partial z^2} - i\mathcal{B}_{ab}\frac{\partial}{\partial z} + \mathcal{C}_{ab}\right) f_b(z) = E f_a(z). \tag{3}$$

The matrix coefficients $\mathcal{A}, \mathcal{B}, \mathcal{C}$ in Eq. (3) are assumed to be constant in each layer. In a heterostructure the differences in the band-edge energies give rise to the confining potentials experienced by the carriers.

Equation (3) is solved by the use of the finite-element method (FEM) for symmetric as well as for asymmetric quantum wells. It has been shown that FEM can

be adapted to yield very accurate eigenvalues for bound-state problems,[11,12] and for obtaining solutions of problems with complex geometries in quantum semiconductor heterostructures.[13,14] In FEM, the heterostructure layers are split up into a number of "cells" or elements, in each of which the physical considerations of the problem hold. The eigenvalue problem, Eq. (1), is set up in each element by assuming that the wave functions are given locally in each element by fifth-order Hermite interpolation polynomials, which have the property that the expansion coefficients correspond to the values of the wave function and its derivatives at select points, called nodes, in the element. The global wave functions $f_i(z)$ are constructed by joining the locally defined interpolation functions and matching the function and its derivative across the element boundary for each of the bands included in the analysis. The *heterointerface* boundary conditions consisting of continuity of the functions and of the *probability current*, and the boundary conditions for the bound states at $z = \pm\infty$ are readily incorporated into the FEM. The element matrices are overlaid into a global matrix in a manner consistent with the boundary conditions. The resultant global eigenvalue problem is a generalized eigenvalue problem which is solved for the eigenenergies and wave functions with a standard diagonalizer on a workstation. Additional details will be given elsewhere.[15]

The use of three elements per layer leads to very accurate quantum-well energies and eigenfunctions in the FEM. The eigenvalues agree with those obtained from the eight-band transfer-matrix method[16–19] to within 10^{-6} eV; the results can be obtained with double precision accuracy by employing more elements in the computation.

B. Quasibound states

In this section we demonstrate that quasibound states occur for energies between the upper and lower barrier potential as depicted in Fig. 1. We begin by presenting a simple one-band model of quasibound states to aid the reader in understanding the experimental results. Following a modification of Messiah's treatment,[9] we define the wave function $\psi(z)$ for energies E, such that $V_1 < E < V_3$ as

$$\psi(z) = \begin{cases} e^{ik_1 z} + re^{-ik_1 z}, & -\infty < z \le 0 \\ 2A\sin(k_2 z + \phi), & 0 \le z \le d \\ 2Be^{-k_3(z-d)}, & d \le z < \infty, \end{cases} \tag{4}$$

where k_1, k_2, and k_3 are wave vectors of the carrier in the three regions defined in Fig. 1. We define the occupancy $\Omega(E)$ to be the probability of a carrier being present within the well region:

$$\Omega(E) \equiv \int_0^d |\psi(z)|^2\, dz$$

$$= |A|^2 \left[2d - \frac{1}{k_2}\{\sin(2\alpha) - \sin(2\phi)\}\right], \tag{5}$$

where $\alpha = k_2 d + \phi$, $|A|^2$ and ϕ are given by

$$|A|^2 = \left[1 + \left\{\left(\frac{k_2 m_1^*}{k_1 m_2^*}\right)^2 - 1\right\}\cos^2\phi\right]^{-1}, \tag{6}$$

$$\phi = -k_2 d + \tan^{-1}\left(-\frac{k_2 m_3^*}{k_3 m_2^*}\right). \tag{7}$$

We take the energies at which $\Omega(E)$ has local maxima to be those corresponding to quasibound states. These quasibound state energies roughly correspond to the energy at which half-integer multiples of the particle wavelength nearly fit within the quantum well.

IV. RESULTS AND DISCUSSION

A. 100-Å-wide quantum wells

We begin by first considering the well-known case of a symmetric single quantum well. Figure 2 shows the piezomodulated reflectivity of the 100-Å symmetric quantum well. Note that the insets shown in this figure, and in all figures to follow, are not a magnification of the main plot but instead are separate scans where the spectrometer slits and the amplifier have been optimized for weak signals. The strongest feature at 1.5156±0.0004 eV is the free exciton from the 0.5-μm-thick GaAs buffer layer on which the quantum well was grown. There is also a feature at 1.494 eV attributed to a residual acceptor associated with a neutral carbon impurity having a binding energy of 25 meV.[20] These two features were present in all samples measured. The Al-Ga-As barrier signature at 1.931 eV allowed calibration of the Al content. The cali-

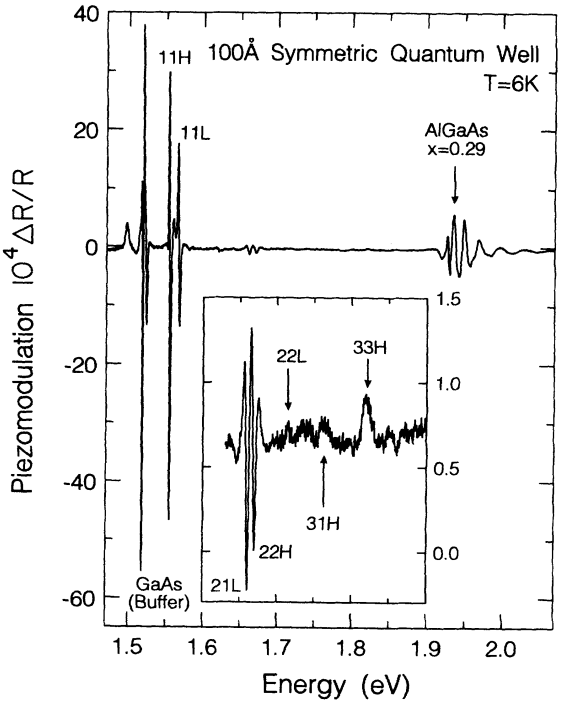

FIG. 2. The piezomodulated reflectivity spectrum of the 100-Å-wide $Al_{0.29}Ga_{0.71}As/GaAs/Al_{0.29}Ga_{0.71}As$ symmetric quantum well at a temperature of $T = 6$ K.

bration was achieved by utilizing the expression of Bosio *et al.*[21] for the excitonic energy gap of Al-Ga-As vs Al concentration. Both the experimentally determined and the theoretically predicted transition energies according to the three-band bound-state model are presented in Table I. For labeling the transitions we use a notation in which the first number indicates the conduction-band state and the second the valence-band state, with H and L identifying hh and lh states. Any transitions which involve quasibound states are denoted by a superscript q after the number. Note that all the theoretical values are uncorrected for excitonic binding energies. The calculations were carried out with the assumption that the well width is an integral multiple of half the lattice constant of GaAs ($a = 5.65$ Å) and with the conduction-band offset taking up 60% of the total band offset. The theory predicted five hh states of which three were observed and three lh states of which we observed two. Transitions involving all three predicted conduction-band states were observed.

As shown in Fig. 2, the Al-Ga-As barrier signature above 1.9 eV contains many features. This complex structure may arise due to a number of possibilities. The stronger features in the vicinity of 1.931 eV are most likely due to a slight difference in composition of the two barrier layers, one on each side of the quantum well. The weaker features at energies above 1.931 eV may be due to above-barrier resonances in symmetric quantum wells described by Bastard[2] and Bastard *et al.*[3] In addition to above-barrier resonances, transitions from the Γ_7 spin-orbit split-off band to the Γ_6 conduction band are also expected in the region above 1.931 eV.[7]

The 100-Å asymmetric single quantum well was grown with unequal barrier heights corresponding to Al concentrations of $x_1 = 0.14$ and $x_3 = 0.31$ as determined from the barrier signatures shown in Fig. 3. The lowering of one barrier causes a few of the bound states in the symmetric case to become quasibound. The number of bound states is reduced to two conduction-band states, three hh states, and two lh states. The plot of the occupancy $\Omega(E)$ in Fig. 4 shows two quasibound hh states and one quasibound lh state, as well as one quasibound conduction-band state, thus accounting for the missing bound states from the symmetric quantum well due to the lowered barrier height. Each of the quasibound

TABLE I. Transition energies (eV) for the 100-Å symmetric well. Note that the theoretical values are uncorrected for excitonic binding energies. A well width of 101.76 Å was used for the calculations.

Expt.	Theory	Identification
1.551	1.558	$11H$
1.563	1.573	$11L$
1.656	1.658	$21L$
1.663	1.665	$22H$
1.712	1.716	$22L$
1.761	1.757	$31H$
1.817	1.814	$33H$

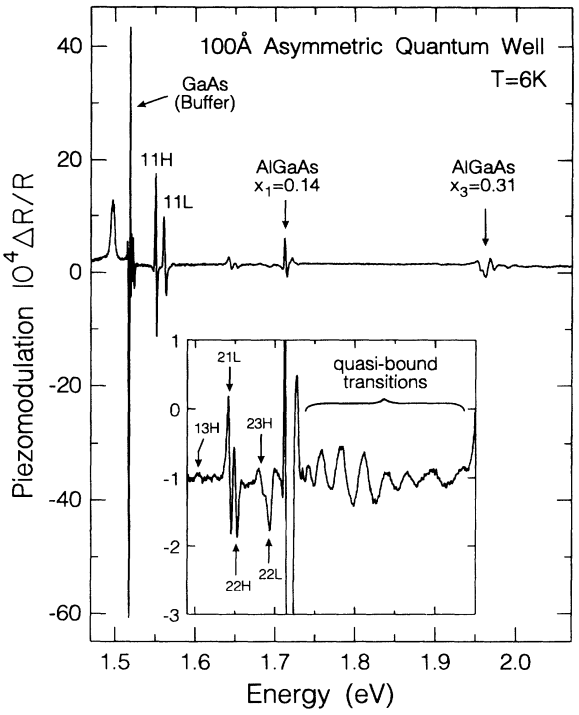

FIG. 3. The piezomodulated reflectivity spectrum of the 100-Å-wide $Al_{0.14}Ga_{0.86}As/GaAs/Al_{0.31}Ga_{0.69}As$ asymmetric quantum well at $T = 6$ K.

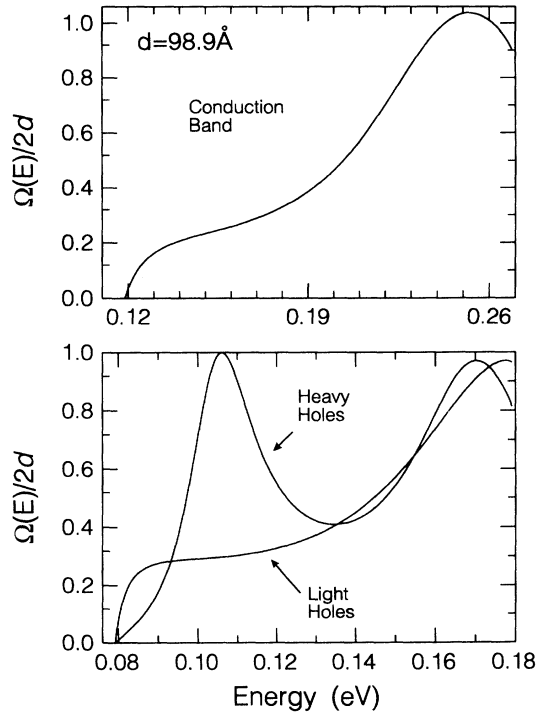

FIG. 4. A plot of the occupancy $\Omega(E)/2d$ defined in Eq. (5) as a function of energy for the conduction and valence bands of the 100-Å-wide asymmetric quantum well. The energy is measured with respect to the GaAs band edge and ranges from the lower barrier energy to the upper barrier energy.

states appears at a slightly lower energy than its bound counterpart in the symmetric quantum well. The experimental and theoretical transition energies are shown in Table II. The transitions involving quasibound states are easily seen between the two barrier signatures.

For this particular sample, bound to quasibound state transition energies are expected below the lower barrier signature. However, they are expected to appear too close to the more intense bound to bound transitions to allow observation.

B. 50-Å-wide quantum wells

We now turn to the interpretation of the piezomodulated reflectivity spectrum of the symmetric 50-Å-wide single quantum well shown in Fig. 5. The barrier signature at 1.932 eV corresponds to an Al concentration of $x = 0.29$. We wish to note the labeling of two peaks as $11H$ transitions; the small $11H$ transition, 5.2 meV lower in energy than the larger $11H$ transition, is attributed to a transition corresponding to a region within the sample containing a quantum well one monolayer wider than the region giving rise to the larger $11H$ transition. The widths of the two regions were deduced from the theoretical model to be 48.1 and 50.9 Å. This effect is often observed in heterostructures grown with growth interruptions.[22–24] The calculations based on a well width of 48.1 Å predict two quantum-confined levels in the conduction band as well as two hh and lh bound states in the valence band. Transitions involving all the theoretically predicted bound states are observed and their transition energies are presented in Table III.

The asymmetric 50-Å quantum well shown in Fig. 6 shows fewer transitions involving quasibound states than does the 100-Å asymmetric well in Fig. 3. This may

TABLE II. Transition energies (eV) for the 100-Å asymmetric well. Note that the theoretical values are uncorrected for excitonic binding energies. A well width of 98.9 Å was used for the calculations.

Expt.	Theory	Identification
1.548	1.554	$11H$
1.559	1.568	$11L$
1.601	1.608	$13H$
1.641	1.645	$21L$
1.648	1.652	$22H$
1.678	1.685	$23H$
1.691	1.695	$22L$
1.732	1.725	13^qL
	1.730	24^qH
1.742		
1.739	1.779	3^q1H
1.782	1.793	3^q1L
	1.794	25^qH
	1.800	3^q2H
	1.802	23^qL
1.809	1.833	3^q3H
1.835	1.843	3^q2L
1.859	1.878	3^q4^qH
1.894		

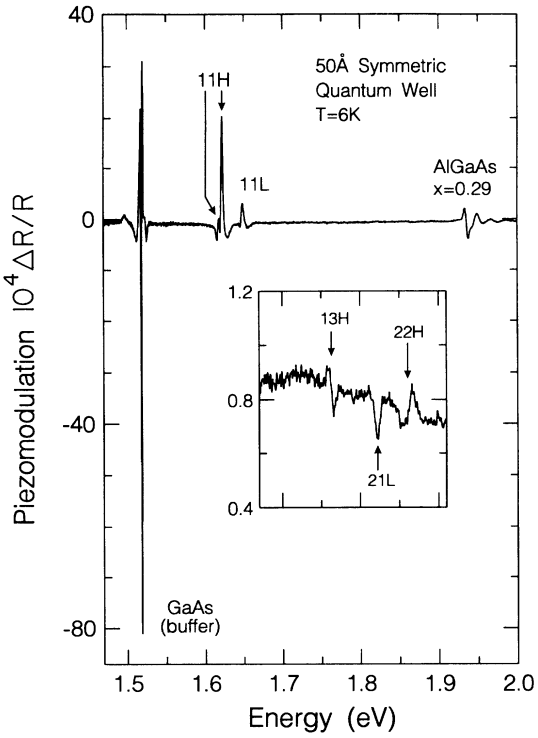

FIG. 5. The piezomodulated reflectivity spectrum of the 50-Å-wide $Al_{0.29}Ga_{0.71}As/GaAs/Al_{0.29}Ga_{0.71}As$ symmetric quantum well at $T = 6$ K. The smaller feature labeled $11H$ is a $11H$ transition attributed to a region within the sample which is one monolayer larger than the remainder of the sample.

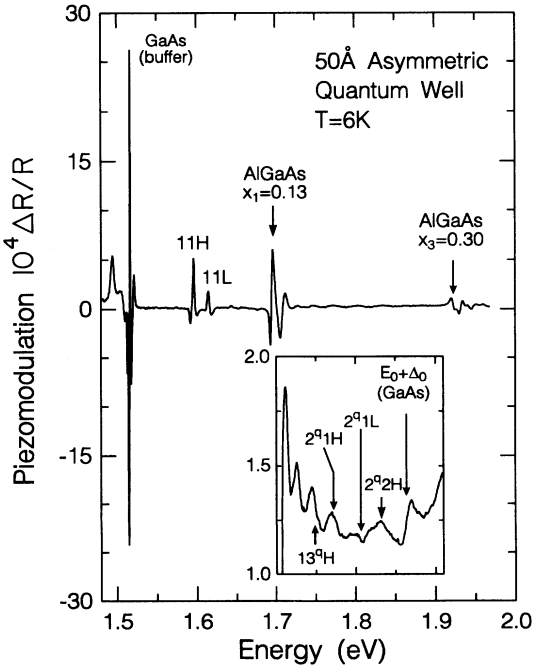

FIG. 6. The piezomodulated reflectivity spectrum of the 50-Å-wide $Al_{0.13}Ga_{0.87}As/GaAs/Al_{0.30}Ga_{0.70}As$ asymmetric quantum well at $T = 6$ K.

TABLE III. Transition energies (eV) for the 50-Å symmetric well. Note that the theoretical values are uncorrected for excitonic binding energies. A well width of 48.1 Å was used for the calculations.

Expt.	Theory	Identification
1.619	1.627	$11H$
1.646	1.659	$11L$
1.761	1.767	$13H$
1.819	1.823	$21L$
1.860	1.859	$22H$

be directly correlated with the occupancy plot in Fig. 7. For energies between the barriers the lh states lack a true maximum, and both the hh states and the conduction-band states show one quasibound state. Hence, there are only two quasibound states available for optical transitions. The bound states consist of two hh states and one lh state in the valence band, and one conduction-band state. There is one unexplained feature at 1.727 eV which may be associated with the Al-Ga-As lower barrier signature. In this sample we were able to observe the transition at 1.859 eV from the spin-orbit split-off band to the conduction band in the GaAs buffer. The experimental and theoretical transition energies are shown in Table IV.

TABLE IV. Transition energies (eV) for the 50-Å asymmetric well. Note that the theoretical values are uncorrected for excitonic binding energies. A well width of 50.9 Å was used for the calculations.

Expt.	Theory	Identification
1.596	1.602	$11H$
1.615	1.626	$11L$
1.644	1.652	$12H$
1.727		
1.747	1.747	13^qH
1.772	1.785	2^q1H
1.799	1.809	2^q1L
1.829	1.835	2^q2H

C. 33-Å-wide quantum wells

The results on the 33-Å-wide symmetric quantum well shown in Fig. 8 provided an opportunity to experimentally determine the excitonic binding energy of the $11H$ and $11L$ transitions. On the high-energy side of the $11H$ and $11L$ peaks, smaller signatures corresponding to the $2s$ excitonic transitions are unambiguously resolved. The $2s$-$1s$ splittings are 11.0 and 11.5 meV for the $11H$ and $11L$ transitions, respectively. One must be aware of the possibility that these features may arise from a monolayer fluctuation of the quantum-well width, as in the case of the 50-Å-wide symmetric quantum well. Decreas-

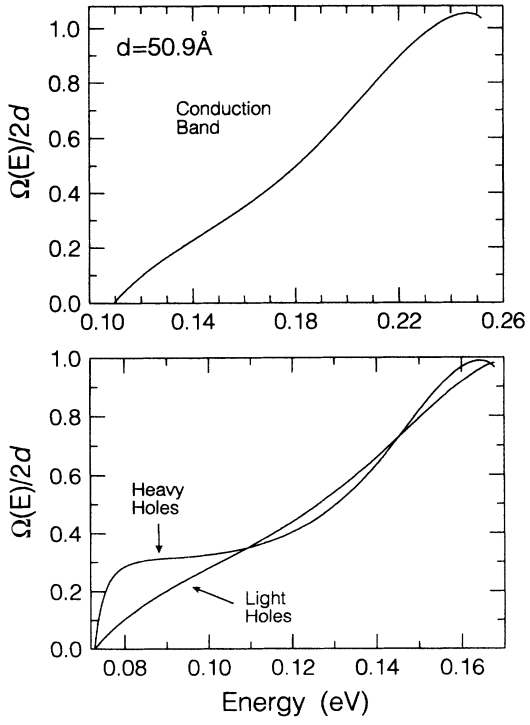

FIG. 7. A plot of the occupancy $\Omega(E)/2d$ as a function of energy for the conduction and valence bands of the 50-Å-wide asymmetric quantum well. The energy is measured with respect to the GaAs band edge and ranges from the lower barrier energy to the upper barrier energy.

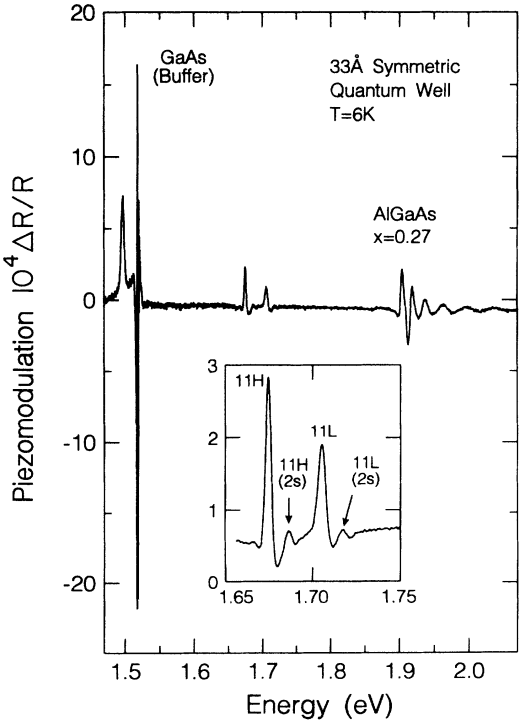

FIG. 8. The piezomodulated reflectivity spectrum of the 33-Å-wide $Al_{0.27}Ga_{0.73}As/GaAs/Al_{0.27}Ga_{0.73}As$ symmetric quantum well at $T = 6$ K.

TABLE V. Transition energies (eV) for the 33-Å symmetric well. Note that the theoretical values are uncorrected for excitonic binding energies. A well width of 31.1 Å was used for the calculations.

Expt.	Theory	Identification
1.672	1.684	$11H$-$1s$
1.683		$11H$-$2s$
1.703	1.723	$12L$-$1s$
1.714		$11L$-$2s$

ing the well width by one monolayer would shift the transition energies by 14.7 and 15.5 meV for the $11H$ and $11L$ transitions. The resolution of piezomodulated reflectivity (± 1 meV) is sufficient to rule out this possibility. Hence we are able to determine the excitonic binding energy by multiplying the $2s$-$1s$ splitting by $\frac{4}{3}$ to get 14.7 and 15.3 meV for the $11H$ and $11L$ transitions, respectively. These values correlate well with previously published results.[25] The observed transitions indicate there is just one bound state for the conduction band and one hh and one lh bound state. However, the theoretical model predicts a second hh bound state just 12 meV below the barrier which may not be sufficiently bound to be observed. Table V presents the theoretical and experimental transition energies for the 33-Å symmetric quantum well.

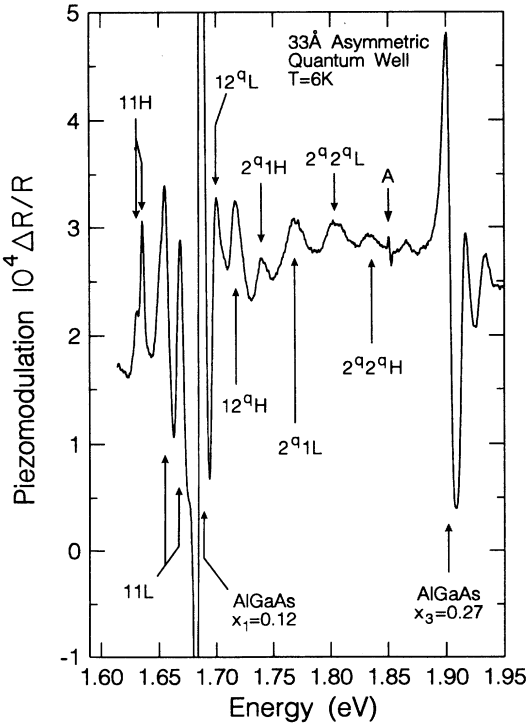

FIG. 9. The piezomodulated reflectivity spectrum of the 33-Å-wide $Al_{0.12}Ga_{0.88}As/GaAs/Al_{0.27}Ga_{0.73}As$ asymmetric quantum well at $T = 6$ K. The $11H$ and $11L$ transitions are assigned to two signatures arising from regions within the sample differing by one monolayer. Note the GaAs signature from the buffer layer has been omitted for clarity.

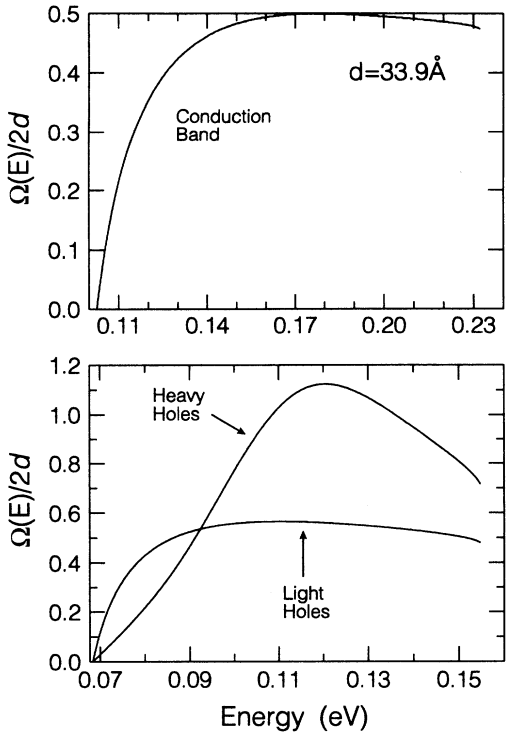

FIG. 10. A plot of the occupancy $\Omega(E)/2d$ as a function of energy for the conduction and valence bands of the 33-Å-wide asymmetric quantum well. The energy is measured with respect to the GaAs band edge and ranges from the lower barrier energy to the upper barrier energy.

The 33-Å asymmetric quantum well is unique in that the number of transitions involving quasibound states, as shown in Fig. 9, is greater than in the wider 50-Å asymmetric quantum well. This is again easily understood by examining the occupancy plot in Fig. 10. The hh, lh, and the conduction band all have one maximum in $\Omega(E)$ corresponding to a quasibound state. In contrast, the wider 50-Å quantum well possessed no quasibound lh states. The widths of the occupancy maxima are very large, and this introduces a considerable uncertainty in the theoretical predictions of the transition energies shown in Table VI. The bound to bound state $11H$ and $11L$ tran-

TABLE VI. Transition energies (eV) for the 33-Å asymmetric well. Note that the theoretical values are uncorrected for excitonic binding energies.

Expt.	Theory	Identification	Well width (Å)
1.628	1.636	$11H$	33.9
1.633	1.643	$11H$	31.0
1.655	1.661	$11L$	33.9
1.666	1.668	$11L$	31.0
1.695	1.714	12^qL	33.9
1.714	1.724	12^qH	33.9
1.732	1.730	2^q1H	33.9
1.760	1.755	2^q1L	33.9
1.801	1.808	2^q2^qL	33.9
1.829	1.818	2^q2^qH	33.9
1.863			

sitions below the lower Al-Ga-As barrier are split into two peaks. This is due to a one-monolayer fluctuation of the well width between 31.0 and 33.9 Å. The sharp feature labeled A in Fig. 9 at 1.849 eV is due to an iodine emission line from the light source and does not originate from the sample.

D. 20-Å-wide quantum wells

The smallest quantum well examined was 20 Å wide. The symmetric quantum well has just one bound state in the conduction band and one hh and one lh bound state in the valence band as shown in Fig. 11. The $11H$ and $11L$ transition energies are at 1.754 and 1.786 eV, respectively. The transition from the GaAs buffer layer spin-orbit split-off band to the conduction band is visible at 1.859 eV.

A symmetric well must have at least two transitions corresponding to $11H$ and $11L$. However, an asymmetric quantum well with unequal barrier heights is not required to possess a bound state. The piezomodulated reflectivity spectrum shown in Fig. 12 shows just one transition from a bound hh state to the bound conduction-band state. There is no bound lh state in this sample. This is demonstrated by the experimental results as well as by the theoretical predictions. The $11H$ transition is just 14 meV below the lower Al-Ga-As valence-band barrier. The missing lh state has become a quasibound state 17 meV above the lower valence-band barrier as shown by the plot of $\Omega(E)$ in Fig. 13. Note that in this sample the hh lacks a true maximum in $\Omega(E)$. In order to adequately explain all features in Table VII, the second hh

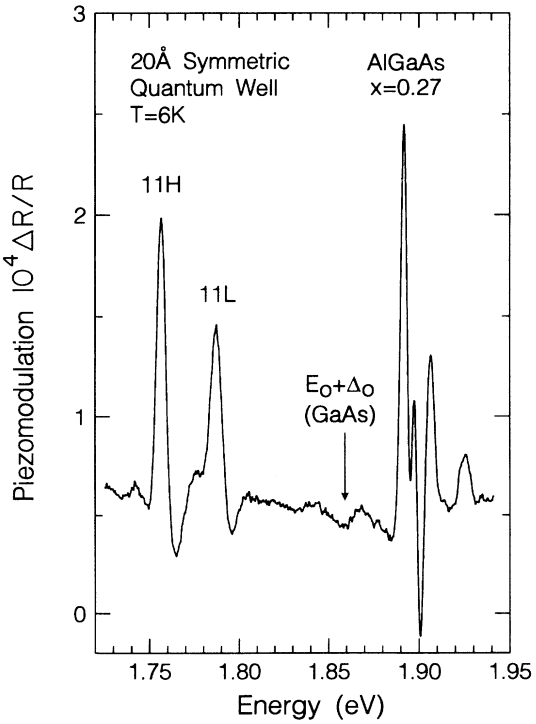

FIG. 11. The piezomodulated reflectivity spectrum of the 20-Å-wide $Al_{0.27}Ga_{0.73}As/GaAs/Al_{0.27}Ga_{0.73}As$ symmetric quantum well at $T = 6$ K. The GaAs buffer layer signature has been omitted for clarity.

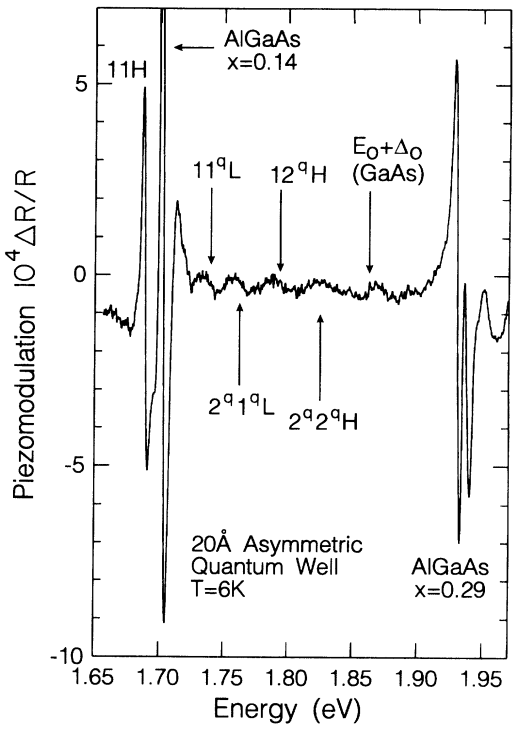

FIG. 12. The piezomodulated reflectivity spectrum of the 20-Å-wide $Al_{0.14}Ga_{0.86}As/GaAs/Al_{0.29}Ga_{0.71}As$ asymmetric quantum well at $T = 6$ K. Note the absence of the $11L$ transition. The GaAs buffer layer signature has been omitted for clarity.

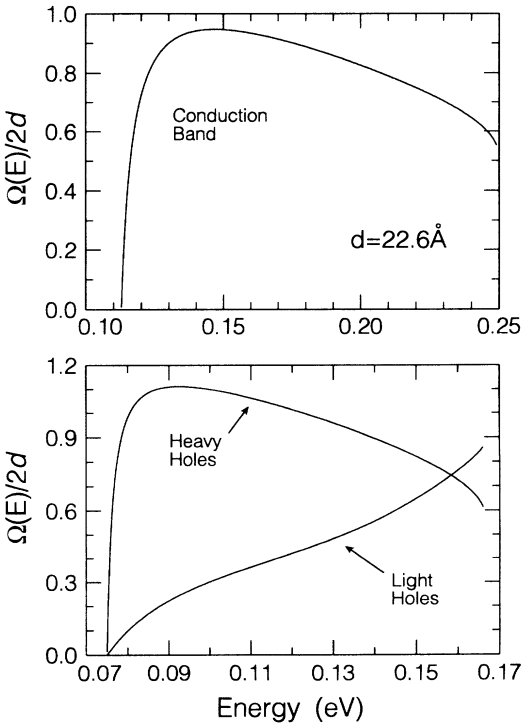

FIG. 13. A plot of the occupancy $\Omega(E)/2d$ as a function of energy for the conduction and valence bands of the 20-Å-wide asymmetric quantum well. The energy is measured with respect to the GaAs band edge and ranges from the lower barrier energy to the upper barrier energy.

TABLE VII. Transition energies (eV) for the 20-Å asymmetric well. Note that the theoretical values are uncorrected for excitonic binding energies. A well width of 19.8 Å was used for the calculations.

Expt.	Theory	Identification
1.685	1.688	$11H$
1.737	1.722	$11^{q}L$
1.763	1.759	$2^{q}1^{q}L$
1.789	1.798	$12^{q}H$
1.829	1.833	$2^{q}2^{q}H$

state ($2^{q}H$) was assigned to the valence-band edge where $\Omega(E)$ reaches its highest value in Fig. 13.

V. CONCLUDING REMARKS

The present investigation shows that some features arise in the electronic energy level scheme of a quantum-well structure as a result of the nature of the quantum-well profile. While the simplicity of the physical considerations and the ease of fabrication have made the square wells the most investigated quantum-well structure, further insights were obtained, for example, with parabolic quantum wells which led to a better determination of band offsets.[7,26] The fabrication of quasiperiodic quantum-well structures, e.g., the Fibonacci superlattices,[27–29] allowed the unusual nature of the electronic and lattice vibrational levels to be experimentally addressed. In our current work, the quasibound states are associated with an asymmetric quantum well. The absence of a bound state in an asymmetric quantum well with appropriately selected design parameters is a case in point.

The asymmetric quantum-well structures that exhibit quasibound states are worth exploring further in the context of photodetection or optical modulators.[30,31] The differences in the photoionization cross section between the symmetric and the asymmetric quantum wells may be significant in such phenomena. The Stark effect of the bound vs the quasibound states is another aspect worthy of consideration.

Interest in asymmetric quantum wells has also been based on the fact that they have second-order optical nonlinear susceptibilities which can be 3 orders of magnitude larger than those of bulk GaAs [$\chi^{(2)}_{\mathrm{GaAs}}$(second-harmonic generation)$\sim 2\times10^{-10}$ m/V, at 10.6 μm]. Recent work has focused on (i) symmetric single quantum wells with inversion asymmetry induced by an electric field applied across the quantum well,[32] (ii) single quantum wells with a step potential at the bottom of the well from a raised band edge in the well arising from the introduction of Al in the GaAs layer,[32,33] and (iii) asymmetric double quantum wells.[34,35] These investigations have focused on intersubband as well as interband transitions which contribute to the nonlinear susceptibility. The compositionally asymmetric single quantum well investigated here is the simplest of structures with a "geometrically-induced" inversion asymmetry. Our estimate for the interband second-order nonlinear susceptibility, i.e., for $\chi^{(2)}_{\mathrm{asym}}$ (second harmonic generation) for a 100-Å asymmetric well with Al concentrations of 0.4 and 0.1 on the two sides is $\sim 6\times10^{-7}$ m/V.[36,37] Further details of this analysis will be presented elsewhere.

ACKNOWLEDGMENTS

We wish to thank Quantum Semiconductor Algorithms (QSA) for the use of their software for energy-level calculations. D.D. has been supported by Digital Equipment Corporation. The investigation at WPI has been supported by the Strategic Defense Initiative of the Innovative Science and Technology Office (SDI-ISTO) administered by the U.S. Naval Research Laboratory under Grant No. N00014-91-K-2027-LRR and the work at Purdue has been supported by the National Science Foundation, Grant No. DMR-89-21717 (C.P., R.G.A., and A.K.R.) and by the Office of Naval Research Grant No. N00014-89-J-1864 (M.R.M.).

[1] T. A. Weber, C. L. Hammer, and V. S. Zidell, Am. J. Phys. **50**, 839 (1982).
[2] G. Bastard, Phys. Rev. B **30**, 3547 (1984).
[3] G. Bastard, U. O. Ziemelis, C. Delalande, M. Voos, A. C. Gossard, and W. Wiegmann, Solid State Commun. **49**, 671 (1984).
[4] J. J. Song, Y. S. Yoon, A. Fedotowsky, Y. B. Kim, J. N. Schulman, C. W. Tu, D. Huang, and H. Morkoc, Phys. Rev. B **34**, 8958 (1986).
[5] J. J. Song, Y. S. Yoon, P. S. Jung, A. Fedotowsky, J. N. Schulman, C. W. Tu, J. M. Brown, D. Huang, and H. Morkoc, Appl. Phys. Lett. **50**, 1269 (1987).
[6] Y. R. Lee, A. K. Ramdas, F. A. Chambers, J. M. Meese, and L. R. Ram-Mohan, Appl. Phys. Lett. **50**, 600 (1987); Proc. SPIE **794**, 105 (1987).
[7] Y. R. Lee, A. K. Ramdas, A. L. Moretti, F. A. Chambers, G. P. Devane, and L. R. Ram-Mohan, Phys. Rev. B **41**, 8380 (1990).
[8] D. Dossa, L. C. Lew Yan Voon, L. R. Ram-Mohan, C. Parks, R. G. Alonso, A. K. Ramdas, and M. R. Melloch, Appl. Phys. Lett. **59**, 2706 (1991).
[9] L. D. Landau and E. M. Lifshitz, *Quantum Mechanics-Nonrelativistic Theory* (Pergamon, New York, 1958), p. 63; A. Messiah, *Quantum Mechanics* (North-Holland, New York, 1964), Vol. I, p. 88.
[10] G. Bastard, *Wave Mechanics Applied to Semiconductor Heterostructures* (Les Editions de Physique, Les Ulis, France, 1988).
[11] L. R. Ram-Mohan, S. Saigal, D. Dossa, and J. Shertzer, Comput. Phys. **4**, 50 (1990).

[12] J. Shertzer, L. R. Ram-Mohan, and D. Dossa, Phys. Rev. A **40**, 4777 (1989).
[13] J. Shertzer and L. R. Ram-Mohan, Phys. Rev. B **41**, 9994 (1990).
[14] L. R. Ram-Mohan and J. Shertzer, Appl. Phys. Lett. **57**, 282 (1990).
[15] L. R. Ram-Mohan (unpublished).
[16] L. R. Ram-Mohan, K. H. Yoo, and R. L. Aggarwal, Phys. Rev. B **38**, 6151 (1988).
[17] K. H. Yoo, R. L. Aggarwal, and L. R. Ram-Mohan, J. Vac. Sci. Technol. A **7**, 415 (1989).
[18] K. H. Yoo, L. R. Ram-Mohan, and D. F. Nelson, Phys. Rev. B **39**, 12 808 (1989).
[19] B. Chen, M. Lazzouni, and L. R. Ram-Mohan, Phys. Rev. B **45**, 1204 (1992).
[20] C. E. C. Wood, in *Molecular Beam Epitaxy and Heterostructures*, edited by L. L. Chang and K. Ploog (Nijhoff, Dordrecht, The Netherlands, 1985), p. 149; A. Y. Cho, *ibid.*, p. 191.
[21] C. Bosio, J. L. Staehli, M. Guzzi, G. Burri, and R. A. Logan, Phys. Rev. B **38**, 3263 (1988).
[22] T. Hayakawa, T. Suyama, K. Takahashi, M. Kondo, S. Yamamoto, S. Yano, and T. Hijikata, Appl. Phys. Lett. **47**, 952 (1985).
[23] R. C. Miller, C. W. Tu, S. K. Sputz, and R. F. Kopf, Appl. Phys. Lett. **49**, 1245 (1986).
[24] R. F. Kopf, E. F. Schubert, T. D. Harris, and R. S. Becker, Appl. Phys. Lett. **58**, 631 (1991).
[25] D. F. Nelson, R. C. Miller, C. W. Tu, and S. K. Sputz, Phys. Rev. B **36**, 8063 (1987).
[26] R. C. Miller, A. C. Gossard, D. A. Kleinman, and O. Munteanu, Phys. Rev. B **29**, 3740 (1984).
[27] R. Merlin, K. Bajema, Roy Clarke, F.-Y. Juang, and P. K. Bhattacharya, Phys. Rev. Lett. **55**, 1768 (1985).
[28] M. Nakayama, H. Kato, and S. Nakashima, Phys. Rev. B **36**, 3472 (1987).
[29] D. J. Lockwood, A. H. MacDonald, G. C. Aers, M. W. C. Dharma-wardana, R. L. S. Devine, and W. T. Moore, Phys. Rev. B **36**, 9286 (1987).
[30] B. F. Levine, C. G. Bethea, K. K. Choi, J. Walker, and R. J. Malik, J. Appl. Phys. **64**, 1591 (1988).
[31] G. Hasnain, B. F. Levine, D. L. Sivco, and A. Y. Cho, Appl. Phys. Lett. **56**, 770 (1990).
[32] M. M. Fejer, S. J. B. Yoo, R. L. Byer, Alex Harwit, and J. S. Harris, Jr., Phys. Rev. Lett. **62**, 1041 (1989); S. J. B. Yoo, M. M. Fejer, R. L. Byer, and J. S. Harris Jr., Appl. Phys. Lett. **58**, 1724 (1991).
[33] P. Bois, E. Rosencher, J. Nagle, E. Martinet, P. Boucaud, F. H. Julien, D. D. Yang, and J-M. Lourtioz, Superlatt. Microstruct. **8**, 369 (1990); E. Rosencher and Ph. Bois, Phys. Rev. B **44**, 11 315 (1991).
[34] J. Khurgin, Appl. Phys. Lett. **51**, 2100 (1987); Phys. Rev. B **38**, 4056 (1988).
[35] Y. L. Xie, Z. H. Chen, D. F. Cui, S. H. Pan, D. Q. Deng, Y. L. Zhou, H. B. Lu, Y. Huang, S. M. Feng, and G. Z. Yang, Phys. Rev. B **43**, 12 477 (1991).
[36] L. C. Lew Yan Voon, and L. R. Ram-Mohan (unpublished).
[37] D. Dossa, L. C. Lew Yan Voon, L. R. Ram-Mohan, and A. K. Ramdas, Bull. Am. Phys. Soc. **36**, 650 (1991).

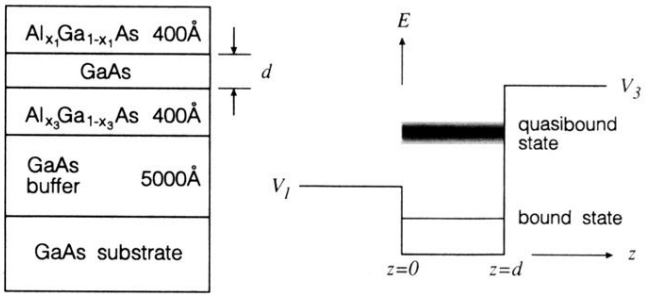

FIG. 1. A plot of the potential profile of an asymmetric $Al_{x_1}Ga_{1-x_1}As/GaAs/Al_{x_3}Ga_{1-x_3}As$ single quantum well.